A proposed model in the analysis of wet pressing

J. C. Roux* and J. P. Vincent

Research engineer and Senior engineer, Centre Technique de L'Industrie Des Papiers, Cartons et Celluloses, D.U. BP 7110, 38020 Grenoble Cedex, France

ABSTRACT *The wet pressing process offers economic advantages in terms of saving energy. We studied the hydromechanical behavior of fiber mats under stress, and this study revealed the importance of pore distribution in the paper sheet. Our pressing model assumes the form of a distributed parameter system for which a numerical method has been developed. The numerical simulations are corroborated by various experimental results published in related literature.*

KEYWORDS
Analysis
Dewatering
Simulations
Wet Pressing

In paper manufacturing, the dewatering process currently involves three stages:

1. Drainage on the sheet-forming units
2. Mechanical water removal in the press sections
3. Evaporation of water from the sheet during drying.

The cost of the energy required for drying may be from 8 times to 20 times that needed for pressing (*1*). Hence, the moisture content of the web as it leaves the last press must be as low as possible, while still meeting the requirements of the finished product.

In wet pressing, an extremely thin sheet of wet paper travels through a press nip. In simple terms, a press nip consists of two rolls, one on top of the other. The water eliminated by this mechanical process is collected in one or two felts.

Wahlstrom (*2, 3*) analyzed the fundamentals of the wet pressing in 1969. His point of view is widely accepted by papermakers, but the quantitative aspects of the wet pressing process have not been studied thoroughly in the context of mathematical modeling. Westra has put forward an analytical model based on a saturated condition, but this model is only partly satisfactory, as Westra himself concludes, because it is difficult to take into account the rewetting phenomena (*4*). We have to mention the didactic rheological models (*5, 6*), as helpful for introducing Wahlstrom's concept of compression-controlled furnishes and flow-controlled furnishes.

More recently, both theoretical and experimental aspects have been developed by Jewett (*7–9*) in an extensive project under contract with the U.S. Dept. of Energy. In this model, the sheet of paper is defined as an unsaturated medium composed of three phases: solids, water, and air. The equation representing the stress-strain relationship for cellulose fiber structures has 7 coefficients identified with a special dynamic compression device (U.M.O. tester) (*10*). The purpose of Jewett's model is to stimulate a transverse-flow press nip.

The models found in the paper industry literature have never taken into account simultaneously (a) the longitudinal flows in the machine direction, (b) the transverse flows through the thickness of the sheet, and (c) the three phases.

In addition, the empirical approach using a regressive model may lead to risky conclusions, if there is too great a departure from identification conditions. Indeed, given the range of variations in the parameters involved in pressing, we believe that only a cognitive model could predict and optimize the wet pressing process under any working conditions whatsoever.

Therefore, we propose a physical analysis to describe the behavior of the wet sheet as a porous medium deformed in the nip. (We have restricted our study to the transverse plane of the sheet: machine direction and thickness.) Since it is not easy to get measurements inside the nip area (*11, 12*), we ran numerical simulations with reference to the two-dimensional velocity field and the two-dimensional pressure field. Among other interesting results, we found the phenomena of rewetting and stratification of the sheet after pressing.

Analysis of the proposed model

When a total stress is applied to a wet sheet in a press, this stress is distributed (a) on the solid structure or

*Presently with: Ecole Francaise de Papeterie et des Industries Graphiques, 461 Rue De La Papeterie—BP 65, 38402 Saint Martin D'Heres Cedex, France.

cellulose fibers, causing varying degrees of deformation and (b) on the two fluid phases—water and air—in the pores, causing hydrodynamic pressures to build up.

The pressure gradients that appear within the structure are thus responsible for flow in the two fluid phases. The problem is one involving isothermic conditions with steady laminar flow within the porous matrix in Euler's description analysis. (These assumptions will be discussed at the end of this paper.)

Intuitively, we recognize that the moisture content of a wet sheet leaving a press nip depends mainly on the compressibility of the solid skeleton and on the resistance to two-phase flow in the porous space between fibers. To get an adequate value of the volumetric fraction represented by porous extra-fiber space or porosity, we need to know the specific volume of the swollen fibers (*7*):

$$\epsilon_s^* = \epsilon_s\,[1 + WRR\,(\rho_s/\rho_l)] = 1 - \epsilon_e \qquad (1)$$

where

WRR = water retention ratio in the intra-fiber porous space
ϵ_s = dry solid volumetric fraction
ϵ_s^* = effective volumetric fraction of the swollen fibers
ρ_s = density of the solid phase
ρ_l = density of the liquid phase
ϵ_e = volumetric fraction of the extra-fiber space, or the volume of void space in the fiber mat.

WRR is assumed to be constant in our analysis.

In the model, we are concerned only with the extra-fiber porous space when dealing with two-phase flow. Thus, the condition of mass conservation leads to the following equation:

$$\epsilon_e = 1 - \frac{(1 - \epsilon_e^0)}{1 + \vec{\nabla} \cdot \vec{s}} \qquad (2)$$

where

ϵ_e^0 = the porosity in the absence of any stresses applied to the wet sheet
$\vec{s}$ = the displacement vector of a solid particle in the deformed sheet related to its location when the sheet is unstressed

$\vec{\nabla} \cdot \vec{s}$ means the relative variation of volume due to the compressibility of the porous space.

When we began the analysis of the hydromechanical behavior of the wet sheet, the general theory of consolidation had been pointed out by Biot (*13*), in 1941, for a saturated porous medium. The papermaker is familiar with this concept, on the basis of the following formulation:

$$P_t = P_s + P_h \qquad (3)$$

where

P_t = total pressure
P_s = structure pressure
P_h = hydraulic pressure.

From Eq. 3, using tensorial notations, we obtain:

$$\bar{\bar{\sigma}}^t = \bar{\bar{\sigma}}^s - P_h \cdot \bar{\bar{\delta}} \qquad (4)$$

where

$\bar{\bar{\delta}}$ = Kronecker's tensor
$\bar{\bar{\sigma}}^t$ = total stresses tensor
$\bar{\bar{\sigma}}^s$ = solid-phase consolidation stresses tensor

To extend this result to the case of a nonsaturated medium, we have included the capillary pressure only in the fraction of porosity where it applied:

$$\bar{\bar{\sigma}}^t = \bar{\bar{\sigma}}^s - P_h\,\bar{\bar{\delta}} - \epsilon_a\,P_c\,\bar{\bar{\delta}} \qquad (5)$$

where

ϵ_a = volumetric fraction of air in the extra-fiber porous space
P_h = air pressure
P_c = capillary pressure, defined by the difference between P_a and P_h.

Apart from this work, Eq. 5 is very close to one found in another analysis (*14*), where the two compressibilities of solid phase χ_s and porous matrix χ_m are included (Eq. 6 in the appendix).

When this analysis is applied to the wet sheet of paper, we are assuming that the porous matrix is not in contact with air and that the solid skeleton is more compressible than the constitutive cellulose fibers:

$$1 - \frac{X_s}{X_m} \qquad (7)$$

Now, to characterize the hydromechanical behavior of the three-phase medium, the balance of forces acting on a small element of sheet may be written as:

1. Statistical analysis

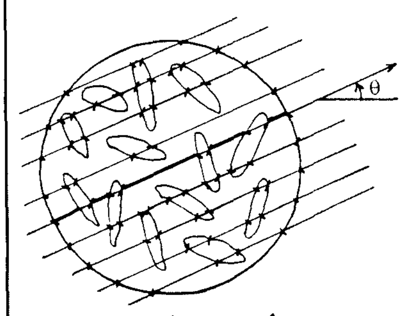

$$\frac{d\epsilon}{d\ell} \simeq \frac{n_i\,\ell_i}{L_e\,\Delta\ell}$$

$$\epsilon \simeq \frac{\sum n_i\,\ell_i}{L_e}$$

$$\vec{\nabla} \cdot \left\{ \bar{\bar{\sigma}}^s - P_h\,\bar{\bar{\delta}} - \epsilon_a\,P_c\,\bar{\bar{\delta}} \right\} = 0 \qquad (8)$$

The wet paper sheet exhibits a complex mechanical behavior: elastic viscoplasticity (*8–10*). Here, the solid skeleton figured by the fibrous network is considered as an orthotropic elastic body. The components of the solid tensor $\bar{\sigma}\epsilon$ may then be related to those of the deformations (spatial derivatives of solid displacement) by the formulation given as Eq. 9 in the appendix.

Using ultrasonic measurements, Habeger has found such a linear relationship and has obtained numerical values of C_{ij} for dry sheets of paper (*15*). The Institut de Mecanique de Grenoble has initiated research to determine the C_{ij} parameters by studying the propagation of ultrasonic waves in a wet sheet considered as an unsaturated porous medium free of any stress (*16*).

When projected in the two main directions adopted, the machine direction (x) and the thickness of the sheet (z), the vectorial equation of equilibrium (Eq. 10 in the appendix) states the consolidation of the web during pressing (*8*).

To complete the model, the conservation of mass flows of the two-fluid phases must also be represented. The particles of each fluid move with a drift velocity $\vec{u}_s$ (*17*):

$$\vec{u}_s = \vec{v}\,(\bar{1} + \frac{\delta \vec{s}}{\delta x}) \qquad (11)$$

2. Spectral distribution of extra-fiber porosity

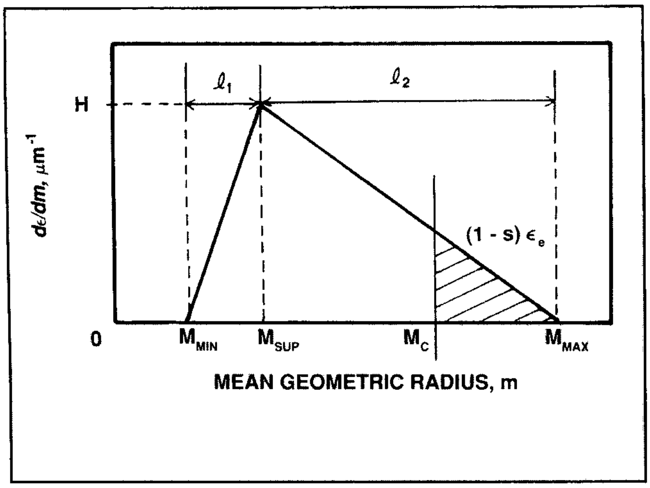

3. Mesh grid of the nip area (15 x 5 points)

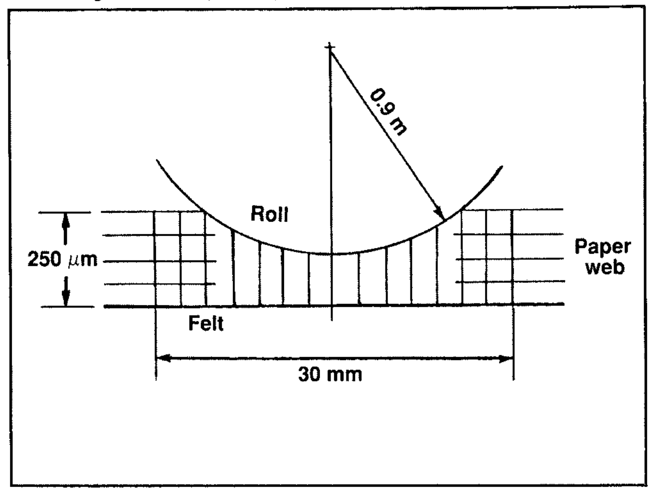

I. Data for the simulations

Web thickness, μm	250
Dry basis weight, g/m^2	70
Water content, kg per kg of dry solid	2.435
Dryness, %	29.1
WRR, kg/kg	0.5
Extra-fiber porosity	0.678
Extra-fiber saturation	0.800
Size, μm	
l_1	1
l_2	5
Specific volume of the swollen particles, m^{-1}	1.51×10^5
Capillary pressure, kPa	3.26
Elastic parameters, mPa	
C_{11}	1360
C_{13}	4.5
C_{33}	10.9
C_{55}	3.2
Anisotropy ratio of permeabilities	1.0
Equivalent radius of the top roll, m	0.900
Speed of the machine	
m/min	600
m/s	10
Max. geometric compression, %	50
Nip length, mm	30

4. Deformation, hydraulic pressure distribution, water flow velocities in the paper sheet in the nip

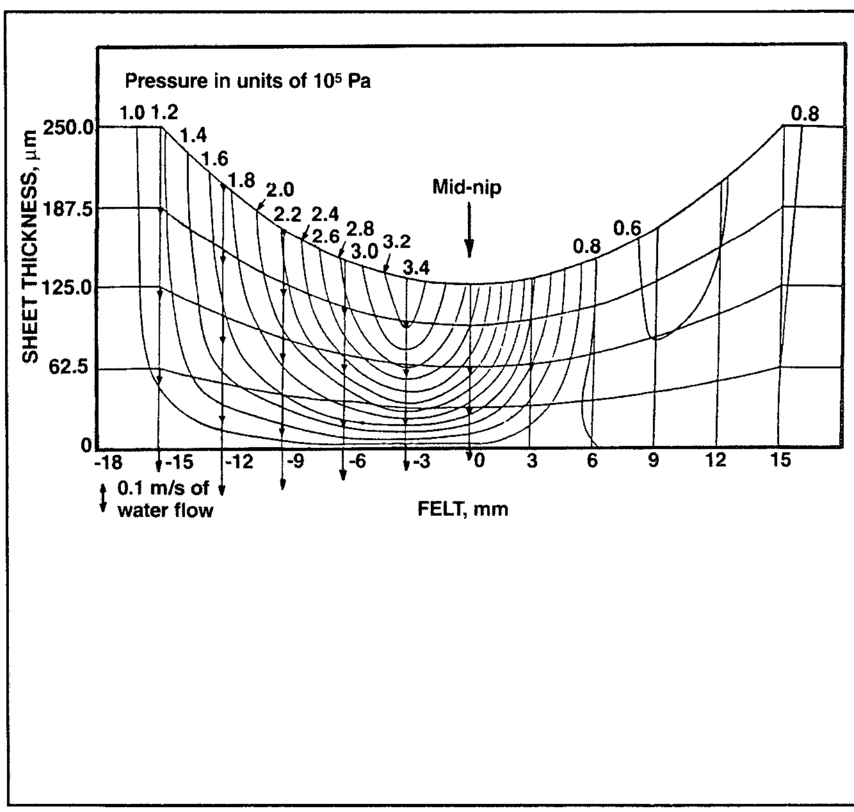

and a relative velocity $\vec{q}_\varphi$ for a phase φ.

Due to the nature of $\vec{u}_s$ (microscopic velocity) and $\vec{q}_\varphi$ (macroscopic velocity) and as Nelson pointed out (*18*), the continuity equations then take the following form:

$$\vec{\nabla} \cdot \left[\rho_\varphi (\epsilon_\varphi \vec{u}_s + \vec{q}_\varphi) \right] = 0 \qquad (12)$$

for water and for air.

The two interstitial fluids are governed by Darcy's law in the interconnected pores of the porous space. However, this is difficult to formulate in this case because of the nonuniform nature of the porous structure.

If we consider a porous medium composed of cylindric capillaries of uniform circular section, Darcy's law in this saturated medium is:

$$\vec{q}_w = -\frac{r^2 \epsilon_e}{k_w \, \mu_w} \, \vec{\nabla} P_h \qquad (13)$$

where r is the radius of a capillary in a uniform porous structure. Taking into account the noncircular section of the capillaries leads us to generalize r by m_h, the so-called mean hydraulic radius (*19*) for a saturated medium:

$$m_h = \epsilon_e / S_v \qquad (14)$$

S_v is the ratio of the area to the volume of a porous medium (in m²/m³) and is a physical parameter of the medium. For capillaries where the mean hydraulic radius lies between m_h and $(m_h + dm_h)$, the corresponding porosity may be written $d\epsilon_e$. These pores contribute to the macroscopic velocity for the water according to Eq. 15:

$$d\vec{q}_w = -\frac{m_h^2\, d\epsilon_e}{k_w\, \mu_w}\, \vec{\nabla} P_h \qquad (15)$$

Assuming now that water is in the "small" pores and air is in the "large" pores, Eqs. 16 and 17 (in the appendix) may be written for each phase (Eq. 16 for water and Eq. 17 for air). In these equations, μ_φ is the dynamic viscosity of a fluid φ and s is the saturation level. The term k φ integrates the relations of dependency between geometry and flows (*20*).

Now, how can we attain the spectral distribution of extra-fiber porosity explicitly included in Eqs. 16 and 17? We could rely on mercury porosimetry measurements to get estimates of $d\epsilon_e/dm_h$, but this was not the method we employed.

Silvy at The Ecole Francaise de Papeterie et des Industries Graphiques has designed a specific method using image analysis of thin sections of wet sheets after displacement of water and consolidation with a low-viscosity resin polymerized *in situ* (*21*). From this specific method, the following parameters may be reached for each pressure level and for each direction θ of statistical analysis (**Fig. 1**) in a plane section of the sheet:

- Porosity ϵ_e
- Specific surface S_v
- Average value of m_h.

A value of 0° for θ indicates the thickness direction, while a value of 90° means the machine direction.

At the beginning of our analysis of wet pressing, we did not dispose of these preceding results, so we had to know precisely how our expressions of permeability account for the decrease with compression.

If we consider the overall porous medium, a characteristic size d is:

$$d = \epsilon_e / S_v \qquad (18)$$

Because it is not easy to deal with the specific volume of the porous medium, we are more interested with the equivalent specific volume of the hydrated solid particles S_0, related to S_v according to Eq. 19:

$$S_v = S_0\,(1 - \epsilon_e) \qquad (19)$$

Taking the assumption that S_0 is a constant value during pressing together with the water retention ratio *WRR* leads to an invariable expression:

$$d(1 - \epsilon_e)/\epsilon_e = d^{\circ}(1 - \epsilon_e^{\circ})/\epsilon_e^{\circ} \qquad (20)$$

So, the two equations, Eqs. 2 and 20, give the reduction of a mean characteristic size d of a porous medium with

5. Hydraulic pressure in each layer of a wet sheet (Layer 1 is near the felt; Layer 5 is near the roll)

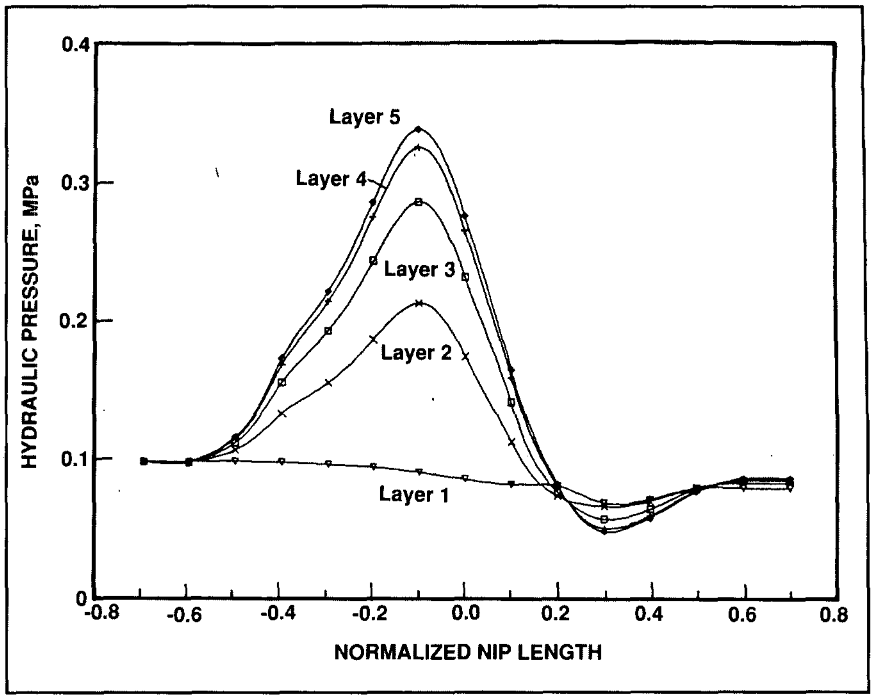

6. Two-dimensional velocity vector field of water flow in the sheet

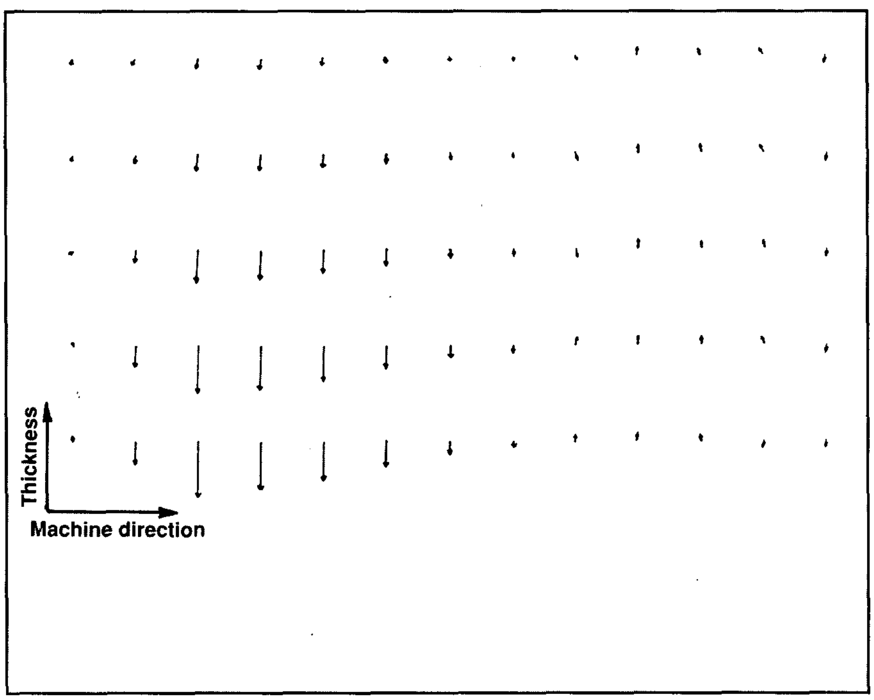

7. Moisture content in each layer of a wet sheet (Layer 1 is near the felt; Layer 5 is near the roll.)

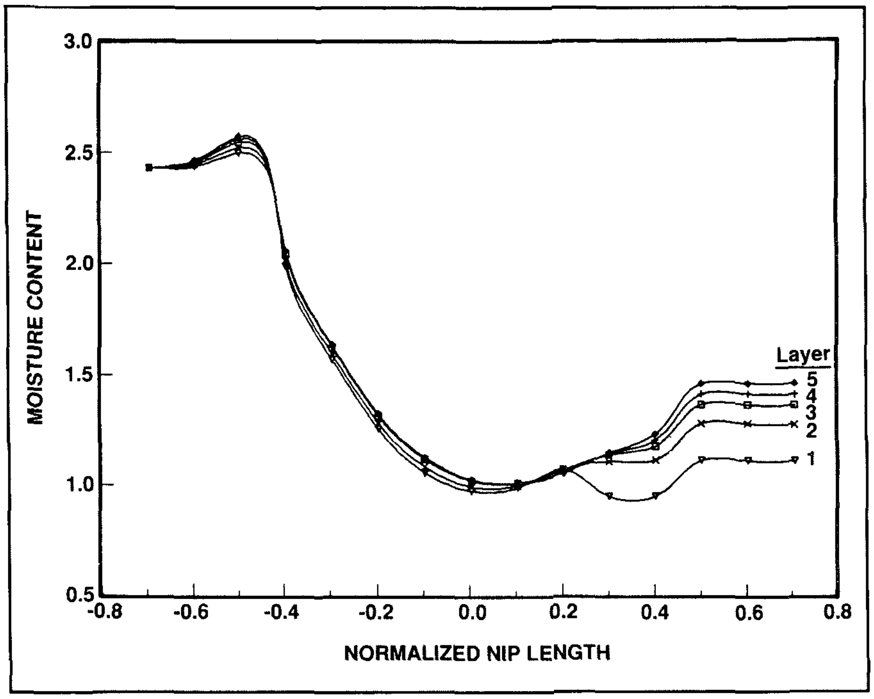

8. Average dryness of a wet sheet during pressing

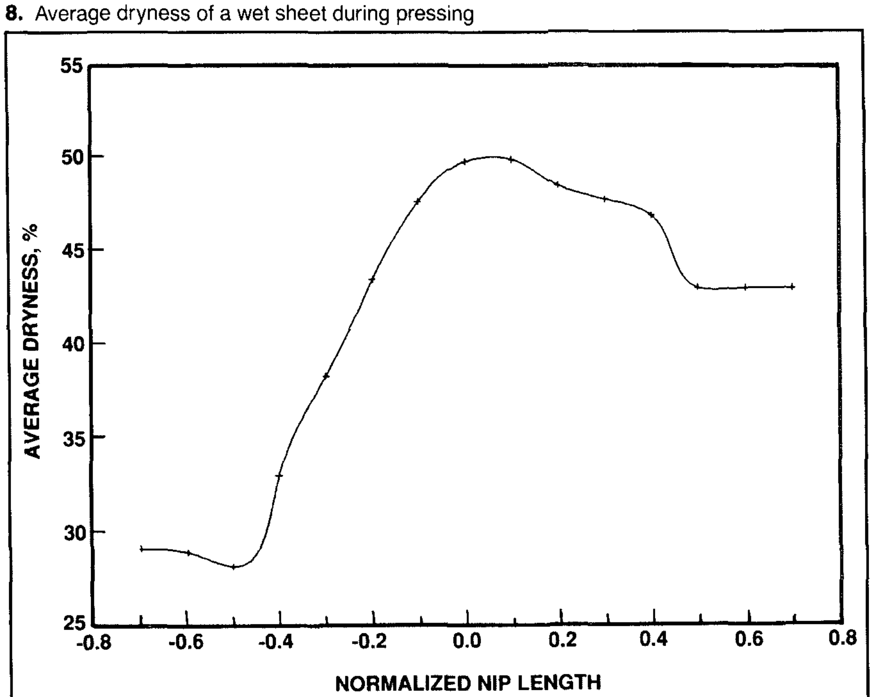

each level of compression during pressing.

We choose the spectral distribution of extra-fiber porosity given in **Fig. 2**: the area of the distribution is exactly ϵ, and l_1 and l_2 are two characteristic sizes of the medium which follow from Eq. 20.

At any point of the wet sheet during pressing, there is a level of saturation s which represents the fraction of porosity occupied by the water.

In Eqs. 16 and 17, the diagonal matrix M takes into account the differences between transverse permeability and in-plane permeability:

$$\bar{\bar{M}} = \begin{bmatrix} 1 & 0 \\ 0 & n \end{bmatrix} \qquad (21)$$

where $(1/n)$ is the anisotropic ratio of the machine direction permeability to the normal permeability through the thickness of the sheet. We have supposed that n was constant during the pressing of the wet sheet. (We will discuss our assumptions at the end of this paper.)

For the computation of the capillary pressure, we have generalized the expression given by Carman (*19*) for a uniform pore distribution:

$$P_c = \gamma \cos \theta / m \qquad (22)$$

to the case of a nonuniform one, given as Eq. 23 in the appendix.

Model integration

The complete model is thus a system of nonlinear partial differential equations in which $\vec{s}$, P_h, ϵ_e are unknowns.

The first equation is a vectorial one pertaining to the consolidation of the sheet of paper as a porous medium:

$$\vec{\nabla} \cdot \bar{\bar{\sigma}}^t = 0 \qquad (24)$$

which gives the displacement vector $\vec{s}$ of each solid particle, after solving it.

Our second equation uses this displacement vector to find the air volumetric fraction ϵ_a in each point of the sheet, as given in Eq. 25 in the appendix. (It is the sum of the continuity expressions for each phase).

We give now an overall view of our simplified analysis of the wet pressing. Before going on, it is necessary to complete the boundary conditions.

In a nip press, the web is in contact with a rigid roll that is assumed to be undeformable and which communicates a known displacement to the web as a function of its geometry. In addition, the fluid particles in contact with the rigid roll have zero relative velocity. While water is effectively eliminated in the converging section of the nip, the web is unfortunately rewetted by the felt in the diverging section. The model must be able to simulate this undesirable effect.

We have indirectly taken into account the felt in considering an infinite permeability in the first part of the nip and a limitation on rewetting by the water at the interface between the felt and the sheet of paper when

II. Paper industry data categories

	Extra-fiber saturation				
y	*0e*	*0.25e*	*0.50e*	*0.75e*	*1.00e*
-0.6	0.802	0.805	0.809	0.811	0.814
-0.5	0.828	0.838	0.848	0.853	0.858
-0.4	0.840	0.853	0.866	0.869	0.873
-0.3	0.843	0.858	0.874	0.875	0.875
-0.2	0.841	0.858	0.875	0.874	0.872
-0.1	0.820	0.839	0.858	0.854	0.849
0.0	0.773	0.790	0.807	0.801	0.793
0.1	0.700	0.706	0.714	0.708	0.700
0.2	0.612	0.610	0.609	0.601	0.594
0.3	0.347	0.469	0.493	0.497	0.502
0.4	0.250	0.342	0.377	0.392	0.407
0.5	0.250	0.320	0.355	0.374	0.394
0.6	0.250	0.319	0.355	0.375	0.394

9. Rewetting moisture content vs. eliminated moisture

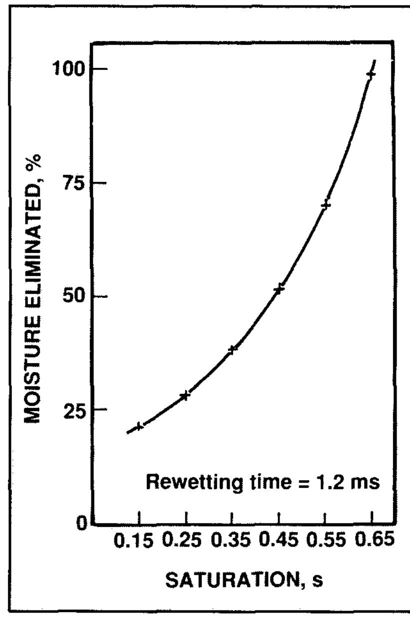

$\partial P_h/\partial y < 0$ in the second part of the nip.

In the simulations presented, we decided to adopt a uniform distribution of porosities ϵ_e and saturations s over the entire thickness of the sheet upline of the nip area.

We shall examine the way in which pressing modifies these values. We have used the finite difference method for programming the two systems, Eqs. 24 and 25, for each point of the mesh grid defined in the paper in **Fig. 3**.

In our model, the nip geometry is the acting parameter which implies all the other conditions prevailing in the nip. In order to solve our problem, we have to progress gradually from an unloaded state to the final geometry of the nip that is achieved at the paper-roll interface.

Since the felt is nonsaturated and incompressible, the equivalent geometry of the nip area is limited by a roll of equivalent radius R_e (which is a function of the radius R_1 and R_2 of the two rolls) and by a plane representing the web-felt interface.

With these working hypotheses, the distribution of stresses in the wet sheet is the result of the movement of the sheet through a defined geometry. For the simulations presented, the data involved are given in **Table I**. These data likely correspond to a low refining level and then to a compression-controlled furnish.

Physical interpretation of results

Figure 4 shows a global representation of these two-dimensional fields obtained by numeric simulations in a compressed sheet of paper: local deformations, isobaric lines of hydraulic pressure, and water flows.

Our elasticity hypothesis leads to a paper thickness after the press equal to the incoming sheet thickness. We know that this is not always realistic, and it would be better to take a plastic behavior for the solid matrix especially for the more refined furnishes (because the plastic deformation of a wet sheet is increasing with its refining level) (*3*). In these cases, we have to modify some of our assumptions: *WRR* and S_0 are not constant values during pressing. This points out some of the limitations in our analysis and some of the difficulties in studying wet pressing!

Another view, in **Fig. 5**, provides the distribution of hydraulic pressure in the compressed sheet. The profiles obtained in this way comply with those found in the literature (*2, 7, 11*).

The hydraulic pressure reaches a maximum before the center line. The center line is indicated by 0 on the x axis, and the normalized nip length extends from -0.5 to + 0.5

The maximum hydraulic pressure is located on the paper-roll interface, and the minimum is located on the paper-felt interface. It appears also that the pressure gradient is zero on the roll side, but in contrast it reaches a maximum on the felt side. Sheet compaction is higher on the felt side as well. This implies a sheet stratification well known by the papermakers and the researchers (*22*), owing to the dynamics of wet pressing. Irreversible deformation is necessary to keep this stratification in the final sheet. Pressure gradients cause the water flow to accelerate from the upper layers toward the lower layers of the web in the converging section of the press nip. **Figure 6** shows the two-dimensional relative velocity vector field (amplitude and direction) of the water flow restricted to the 13 × 5 points in the nip area.

The directions of the velocity vectors are not always vertical, upwards or downwards. The web is wetter near the roll than near the felt, as indicated in **Fig. 7**. This determination also complies with experimental results (*23*). In the diverging part of the nip, a water flow from the felt rewets the sheet, but water from the layers near the felt also rewets with layers near the top roll. The distribution of water is not uniform in the thickness of the sheet.

Figure 8 summarizes these results and shows the mean dryness [dry solid/(dry solid + water)] of the web during pressing. Water eliminated backward from the machine direction leads to a small decrease in the average dryness of 1.5%. Then, the average dryness increases to a maximum of 50.1% after the center line. From this maximum down to 44%, rewetting occurs. Here, we have to mention that our boundary condition at the felt-paper interface (when $\partial P_h / \partial y$ is negative) may be considered a limitation in this problem. Because the felt is not modelized in this analysis, we have to give an indication of the water present in the felt at the interface.

For the nip area, **Table II** gives the distribution of the saturation in the sheet during pressing. On the same working point, we have only changed the saturation level at the felt-paper interface from 0.15 to 0.65. We see in **Fig. 9** for the same rewetting time the dramatic effect of the rewetting phenomenon.

It is not possible to present all the results obtained with our model of the wet pressing. Among other results of interest is the influence of the anisotropic ratio ($1/n$) between in-plane permeability and transverse permeability. We have found a more flow-controlled state when increasing this anisotropic ratio from 1 to 5. With the same moisture content of 2.44 kg/kg before the press, we also noticed a decrease (1%) in the average dryness after the press. Lindsay recently presented measurements of anisotropy and pointed out that the ratio for lateral to transverse permeability was 2-3 in most cases. This ratio does not change significantly with compression in the porosity range of 0.60-0.90 explored (*24*). Our initial choice for this ratio was in the right magnitude.

Conclusions

We have presented a model based only on phyical laws to simulate the pressing of a compression-controlled wet paper sheet. Qualitatively, the various numerical simulations are in close agreement with experimental results already published in the relevant literature. We have also given the limitations of our analysis in this first approach.

We are presently developing a new version of this package with the main aim of integrating the felt model and the nonlinear elastic behavior of the porous media.□

Literature cited

1. Guillet, F., ATIP Revue 39(10): 539(1985);
2. Asklopf, C. A. Larsson, K. O., Linderoth, J., Wahlstrom, P.B., Pulp Paper Mag. Can. 65(6): 246(1964).
3. Wahlstrom, P. B., Pulp Paper Mag. Can 70(19); 76 (1969).
4. Westra, H. A., Paper Technology and Industry 16(3): 165(1975).
5. Carlsson, G. Lindstrom, T., and Norman b., Some basic aspects on west pressing of paper, CPPA/IPC International Water Removal Symposium, Vancouver, 1982, p. 5.
6. Caulfield, D. F., Young, T. L., and Wegner, T. H., Tappi 65(2): 65 (1982).
7. Jewett, K. B. Ceckler, W. H., Busker, L. H., Co A., AIChE Symposium Series 76(200): 59 (1980).
8. Jewett, K. B., A two-phase flow model of a transversal flow press nip, Ph.D. thesis, University of Maine, 1980.
9. Ellis, E. R., experimental work being done at the University of Maine under DOE contract No. EM-78-S-02-4997 as part of his Ph.D. thesis.
10. Ellis, E. R., Compressibility and permeability of never dried bleached softwood kraft pulp and its application to the prediction of wet press, Ph.D. thesis, University of Maine, 1981.
11. Beck, D.A. 1983 Engineering Conference Proceedings, Vol. 2, TAPPI PRESS, Atlanta, P. 475.
12. Beck, D. A., 1986 Engineering Conference Proceedings, TAPPI PRESS, Atlanta, p. 105.
13. Biot, M. A., J. Applied Physics 12: 155(1941).
14. Auriault, J. L., Transport in Porous Media 2(3): 45(1987).
15. Habeger, C. C., Mann, R. W., and Baum, G. A., Ultrasonics 17(2): 57(1979).
16. Lebaigue, O., Determination des caracteristiques hydromecaniques du papier, DEA a l'Institut de Mecanique de Grenoble, 1986.
17. Westra, H. A. and Selling, H.J., Commission of the European Communities, EUR 6679, contract EENL 262-77 (1980).
18. Nelson, R., Tappi 47(12): 752(1964).
19. Carman, P. C., L'ecoulement des gaz a travers les milieux poreux, Bibliotheque des Sciences et Techniques Nucleaires, 1964.
20. Roux, J. C., Modelisation et optimisation du fonctionnement d'une section de presses de machine a papier, These I.N.P., Grenoble, France, 1986.
21. Silvy, J. and Garrido-Yanes, J., Rapport de contrat CTPEFPG (1986).
22. MacGregor, M. A., Tappi J. 66(6): 53(1983).
23. Wicks, L., 1982 Engineering Conference Proceedings, TAPPI PRESS, Atlanta, p. 3.
24. Lindsay, J. D., The anisotropic permeability of paper: theory, measurements and analytical tools, IPC Tech. Paper Series, No. 289, Wisconsin, 1988.

On behalf of Centre Technique du Papier, with its partners Ecole Francaise de Papeterie, Institut de Mecanique de Grenoble, and a group of companies specializing in press construction and operation, the authors acknowledge the financial support of the Agence Française pour la Maîtrise de L' Energie (AFME).

Received for review Jan. 3, 1990.

Accepted July 5, 1990.

Appendix for oversized equations

$$\bar{\bar{\sigma}}^{t} = \bar{\bar{\sigma}}^{s} - \left(1 - \frac{X_s}{X_m}\right) P_h \bar{\bar{\delta}} - P_c \bar{\bar{\delta}} \qquad (6)$$

$$\begin{bmatrix} \overset{s}{\sigma}_{xx} \\ \sigma_{yy} \\ \overset{s}{\sigma}_{xy} \end{bmatrix} = \begin{bmatrix} C_{11} & C_{13} & O \\ C_{13} & C_{33} & O \\ O & O & 2C_{55} \end{bmatrix} \begin{bmatrix} \partial s_x / \partial x \\ \partial s_y / \partial y \\ 1/2\,(\partial s_x \partial y + \partial s_y \partial x) \end{bmatrix} \quad (9)$$

$$C_{11} \frac{\delta^2 s_x}{\delta x^2} + C_{55} \frac{\delta^2 s_x}{\delta z^2} + (C_{13} + C_{55}) \frac{\delta^2 s_z}{\delta x \delta z} - \frac{\delta P_h}{\delta x} - \frac{\delta(\epsilon_a P_c)}{\delta x} = 0$$

$$C_{33} \frac{\delta^2 s_z}{\delta z^2} + C_{55} \frac{\delta^2 s_z}{\delta x^2} + (C_{13} + C_{55}) \frac{\delta^2 s_x}{\delta x \delta y} - \frac{\delta P_h}{\delta y} - \frac{\delta(\epsilon_a P_c)}{\delta y} = 0 \qquad (10)$$

Appendix continued next page >

Appendix for oversized equations (contd.)

$$\vec{q}_w = -\int_0^{s\epsilon_e} \frac{m_h^2\, d\epsilon_e}{k_w(s)\, \mu_w}\, \vec{M}\cdot\vec{\nabla} P_h \qquad (16)$$

$$\vec{q}_a = -\int_{s\epsilon_e}^{\epsilon_e} \frac{m_h^2\, d\epsilon_e}{k_a(s)\, \mu_a}\, \vec{M}\cdot\vec{\nabla} P_a \qquad (17)$$

$$P_c\,(s,\, \epsilon_e) = \frac{\gamma \cdot \cos\theta}{\epsilon_e} \int_{s\epsilon_e}^{\epsilon_e} \frac{d\epsilon_e}{m} \qquad (23)$$

$$\vec{\nabla}\cdot \bar{\bar{\sigma}}' = 0 \qquad (24)$$

$$\vec{\nabla}\cdot(\vec{u}_s + \vec{q}_w + \vec{q}_a) + \frac{(\epsilon_e\, \vec{u}_s + \vec{q}_a)}{P_a}\cdot\vec{\nabla} P_a = 0 \qquad (25)$$